PCCP

Accepted Manuscript

ROYAL SOCIETY OF CHEMISTRY

www.rsc.org/pccp

PCCP

RSCPublishing

ARTICLE

Electrical and thermal transport properties of $Pb_{1-x}Sn_xSe$ solid solution thermoelectric materials

Cite this: DOI: 10.1039/x0xx00000x

Chao-Feng Wu, Tian-Ran Wei, Jing-Feng Li*

Received 00th January 2012,
Accepted 00th January 2012

DOI: 10.1039/x0xx00000x

www.rsc.org/

Both lead selenide (PbSe) and tin selenide (SnSe) are promising thermoelectric compounds consisting of earth-abundant elements, between which solid solutions can be formed in a wide composition range. This study investigated the electrical and thermal transport properties of n-type $Pb_{1-x}Sn_xSe$ (x = 0, 0.01, 0.05, 0.1 and 0.15) solid solutions with an emphasis on the effect of Sn substitution. Small amounts of Sn substitution ($x \leq 0.1$) increased electrical conductivity but showed less influence on Seebeck coefficient, leading to improved power factors, which was revealed to be associated with the generation of native Se vacancies. The electrical conductivity tended to decrease when $x > 0.1$ due to alloying effect, consequently thermoelectric figure of merit was not further increased, even though the thermal conductivity can be reduced with increasing Sn content. A maximum dimensionless figure of merit *ZT* up to 1.0 was obtained at moderate temperature (773K) in the composition of $Pb_{0.9}Sn_{0.1}Se$.

1 Introduction

Thermoelectric (TE) technology enables many applications for power generation and electronic refrigeration, based on the direct conversion between heat and electricity through a solid device.[1] The conversion efficiency is closely associated with the TE material's dimensionless figure of merit, $ZT = S^2\sigma T/\kappa$, where *S* is the Seebeck coefficient, σ the electrical conductivity, *T* the operating temperature in Kelvin, and κ the thermal conductivity. *ZT* enhancement can be achieved through many methods, including carrier density tuning, band engineering, nanostructuring as well as forming solid solutions.[2-4]

Lead selenide (PbSe, space group *Fm-3m*), a direct-gap semiconductor, has been studied for decades mainly with a focus on its excellent optical properties.[5,6] Recently, some investigations have been devoted to its thermoelectric performance[7-17] for its low lattice thermal conductivity and the earth-abundant elemental compositions compared with PbTe, a traditional thermoelectric compound.[8,16,18,19] Raising *ZT* values is the ultimate task, which is of particular importance for new thermoelectric materials including PbSe. Usually forming solid solutions is a general and effective method for *ZT* enhancement, which has been widely applied to well-known SiGe[20] and TAGS[21] alloys used in radioisotope thermoelectric generators (RTGs). However, the formation of solid solutions can also reasonably degrade the TE properties when band structures are not altered, as in the case of PbSe-PbS[22] and PbSe-PbTe[23] systems owing to the impaired carrier mobility. In other words, *ZT* enhancement may be achieved when energy bands are adjusted properly, as demonstrated in a recent study by Wang et al.[24] in PbSe-SrSe alloys, where the net benefit for *ZT* enhancement comes from the band structure tuning other than the thermal conductivity reduction.

The PbSe-SnSe solid solutions with a similarity to PbSe-SrSe exhibit a decreasing band gap at *L* point with increasing Sn content,[25,26] which may lead to some specific performance due to the enhanced interaction between the conduction and valence bands. In this work, we conducted a systematic study on n-type $Pb_{1-x}Sn_xSe$ alloys with $PbCl_2$ dopant for anionic substitution[27] to achieve an optimized doping level of $\sim 4\times10^{19}cm^{-3}$. The transport properties were investigated and explained within the framework of single Kane band (SKB) model which well describes the band structures of PbSe and PbS.[28,29] Relatively high ZT values at moderate temperatures with a maximum value up to 1.0 at 773K were obtained in $Pb_{0.9}Sn_{0.1}Se$ and further increasing the Sn substitution within the investigated compositional range caused little change in thermoelectric properties.

2 Experimental

All samples were fabricated by combining mechanical alloying (MA) and spark plasma sintering (SPS). Pb shots (99.99%, 2-4mm) and elemental powders of Se (99.9%, 75μm) and Sn (99.99%, 75μm) were mixed in nominal compositions of $Pb_{1-x}Sn_xSe$ (x = 0, 0.01, 0.05, 0.1 and 0.15, far lower than the 40 at% solubility limit of SnSe into PbSe[30]), and milled at 450 rpm for 24h in a planetary ball mill filled with high-purity argon gas. 0.1%mol $PbCl_2$ was added to maintain an optimized doping level,[27] and a small amount of excessive Pb (~4%) was added to minimize compensating metal vacancies that led to p-type conduction as well as to improve the mechanical strength.[31] The MA-derived powders were consolidated into disks by SPS at 873K in vacuum for 5min under an axial pressure of 50MPa. Another series of Sn-free compounds were also synthesized via the same processing for evaluating the

doping efficiency of Cl dopant into PbSe, denoted as $Pb_{1.04}Se_{1-y}Cl_y$ with y = 0.002, 0.0025, 0.003 and 0.0035, respectively.

The phase structures of SPS-processed $Pb_{1-x}Sn_xSe$ samples were detected by X-ray diffraction (XRD, D8 Advance A25, Bruker, Germany) using Cu-$K\alpha$ radiation. A field emission scanning electron microscope (SEM, Merlin VP compact, Zeiss, Germany) was employed to investigate the morphology of fractured and polished surfaces. Electro probe micro-analyses (EPMA, JXA-8230, JEOL, Japan) were carried out on the Sn10% sample to validate the elemental distributions of Se, Pb and Sn atoms into the matrix. Direct band gaps of the Sn1%, Sn5% and Sn15% samples were determined through optical measurements (FTIR, Excalibur 3000, Varian, USA). The SPSed samples were cut into bars (~12mm×3mm×3mm) and polished to disks (~ ϕ 10mm × 1mm) for measuring the following thermoelectric properties. The bar samples were used to measure the electrical resistivity and Seebeck coefficient by a Seebeck coefficient/electric resistance measuring system (ZEM-2, Ulvac-Riko, Japan). The Hall coefficients at room and elevated temperatures were collected by the Van der Pauw technique under a reversible magnetic field of 0.52T (8340DC, Toyo, Japan). Thermal diffusivity (λ) measurements were carried out using the disk samples by laser flash technique (TC-9000, Ulvac-Riko, Japan), and the thermal conductivity (κ) was calculated following the equation $\kappa = \lambda D C_P$, where C_p is the heat capacity determined using the equation C_P/k_B per atom = 3.07+4.7×10^{-4} (T/K-300) by fitting experimental data,[32] and D is the density, which was measured through the Archimedes method. The uncertainty of each parameter (Seebeck coefficient, electrical resistivity and thermal conductivity) is estimated to be approximately 5%, leading to a ~20% uncertainty for ZT.

3 Results and Discussion

XRD experiments on SPSed samples showed that nearly a single phase was synthesized by MA and SPS as displayed in Fig. 1(a), where all main peaks can be indexed to a cubic phase of PbSe. Since excessive Pb was added, its peaks were also detected between the PbSe (200) and (220) peaks in all samples.

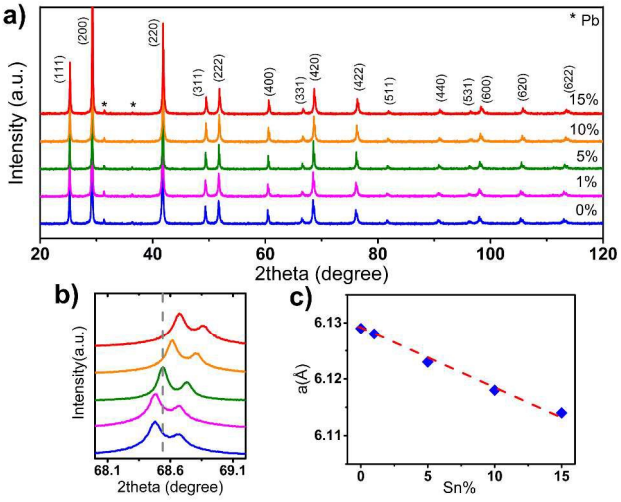

Fig. 1 (a) X-ray diffraction data for $Pb_{1-x}Sn_xSe$ samples. (b) Step-scanning XRD patterns of (420) peaks, and (c) Lattice parameters by extrapolation from high angle peaks, both indicating the formation of $Pb_{1-x}Sn_xSe$ solid solutions.

Sn substitution for Pb resulted in lattice shrinkage, i.e., PbSe Bragg peaks shifting to higher 2θ angles (see Fig. 1(b)), indicating the formation of rocksalt structured $Pb_{1-x}Sn_xSe$ solid solutions.

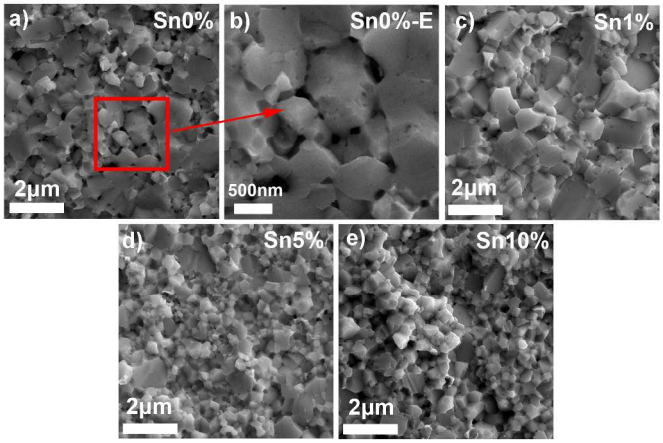

Fig. 2 SEM images for (a) Sn0%, (c) Sn1%, (d) Sn5% and (e) Sn10% samples, respectively. (b) Enlargement of the selected area in (a) Sn0% sample, revealing the existence of nanopores at grain boundaries.

Figures 2(a), (c), (d) and (e) exhibit the SEM morphologies of fractured surfaces for the Sn0%, Sn1%, Sn5% and Sn10% samples, respectively. All the compositions have fine grains with diameters less than one micron, and the grain size tends to be smaller in Sn-rich samples (Sn5% and Sn10%). There were still many nanosized pores at grain boundaries as can be seen from Fig. 2(b), although the relative density was above 94% for all samples. Increased boundaries and nanosized pores scatter both carriers and phonons, but the reduced grain sizes and the existence of nanopores are considered to be thermoelectrically beneficial if the impaired carrier mobility could be compensated by the reduced thermal conductivity.

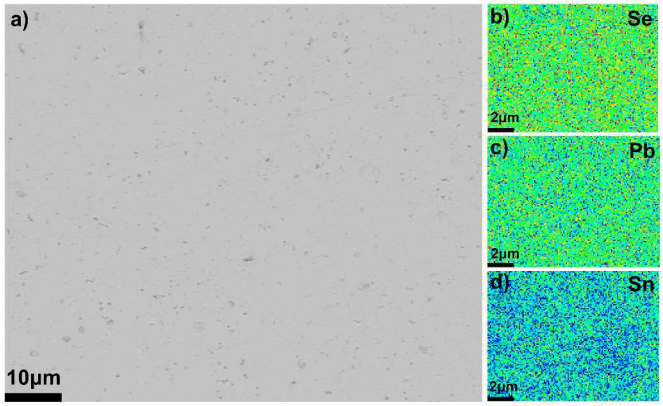

Fig. 3 (a) The back-scattered electron (BSE) image of the Sn10% sample and (b)-(d) EPMA morphologies showing elemental distributions of Se, Pb and Sn in the matrix.

The polished surface of the Sn10% sample showed a homogeneous BSE morphology on a larger scale of 20 micron, where no obvious segregation was detected as shown in Fig. 3(a). The dark spots were ascribed to the pores or polished defects. Localized distributions of Se, Pb and Sn elements also revealed a moderate uniformity throughout the matrix in EPMA

images, indicating satisfactory homogeneity of samples processed by MA and SPS.

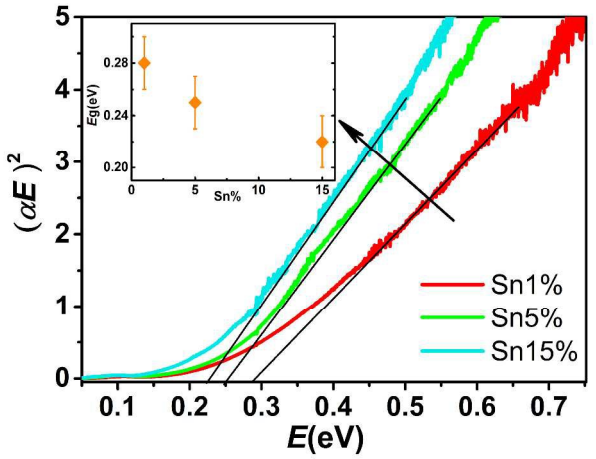

Fig. 4 FTIR results for the Sn1%, Sn5% and Sn15% samples, where α is the absorption coefficient and E the photon energy. The band gap decreased as Sn content increased, with the measured values shown in the inset.

A previous study[26] demonstrated that the $Pb_{1-x}Sn_xSe$ alloys with rocksalt structure exhibit an inversion in band structure, which is known as topological insulators. Calculations[33] on Sn-doped PbSe suggested that when Sn was added into host lattice, the higher Sn-*s* states would push a band out from the host valence band, resulting in a decrease in energy gap at *L* point; however the conduction bands receive less influence because the valence *p* orbits of Sn and Pb are almost the same. FTIR measurements also confirmed that the band gap of pseudobinary $Pb_{1-x}Sn_xSe$ alloys decreased with increasing Sn substitution, as depicted in Fig. 4. The detailed relations between band gap width (E_g) and Sn content (x) or temperature (T) are represented by the equation derived from Strauss's results:[26]

$$E_g = \left[0.13 + (4.5\times10^{-4})\,T/\mathrm{K} - 0.89x\right] \mathrm{eV} \quad (1)$$

The inversion point (here represented by x_c), at which $E_g = 0$ originating from the degeneracy of the L_6^+ and L_6^- band extrema, is deduced to be $x_c = 0.3$ at room temperature, which is somewhat higher than that of $x_c = 0.23$ reported by Dziawa et al. through angle-resolved photoemission spectroscopy (ARPES) studies.[34] In the present work, the Sn substitution was controlled to be lower than the inversion point. Since the decrease of band gap was expected with increasing Sn content, the single Kane band (SKB) model was employed for theoretical predication of thermoelectric transport properties on $Pb_{1-x}Sn_xSe$ systems, with Eqn (1) being taken into account for the determination of band gap via increasing x or T.

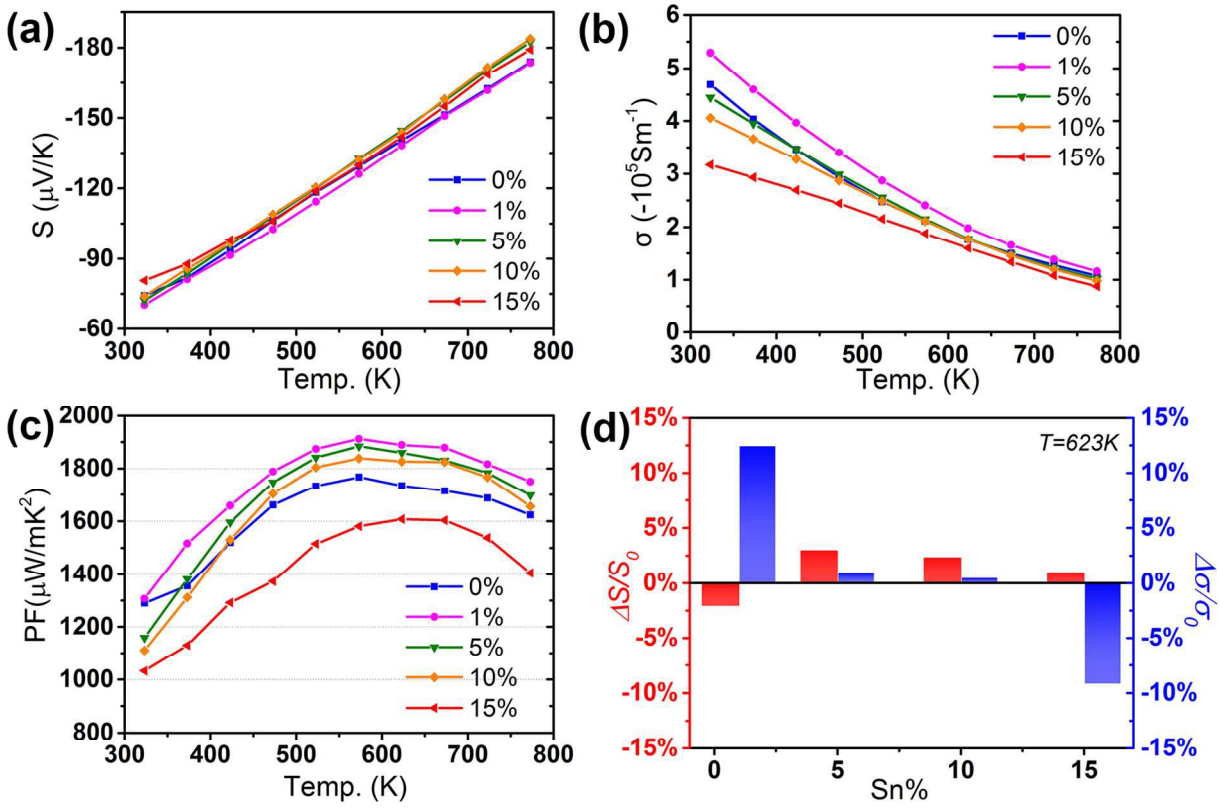

Fig. 5 (a) Seebeck coefficient, (b) Electrical conductivity and (c) Power factor of all $Pb_{1-x}Sn_xSe$ alloys. (d) Variation from the Sn0% sample in Seebeck coefficient and electrical conductivity as a function of Sn content at 623K.

Figures 5(a)-(b) present the thermopower and electrical conductivity, together with the calculated power factor ($PF = S^2\sigma$, Fig. 5(c)) which describes the comprehensive electrical properties of a thermoelectric material. The Seebeck coefficient increased almost linearly with temperature, indicating the strongly degenerate semiconducting behavior of all $Pb_{1-x}Sn_xSe$ samples. Within the SKB model dominated by acoustic phonon scattering, the Seebeck coefficient is expressed as follows:

$$S = \frac{k_B}{e}\left[\frac{{}^1F_{-2}^1}{{}^0F_{-2}^1} - \xi\right] \qquad (2)$$

ξ is the reduced chemical potential $\xi = \mu/k_BT$. In Eqn (2) the integral ${}^nF_l^m$ is defined by the relation:

$${}^nF_l^m = \int_0^\infty (-\frac{\partial f}{\partial \varepsilon})\varepsilon^n(\varepsilon+\alpha\varepsilon^2)^m[(1+2\alpha\varepsilon)^2+2]^{l/2}d\varepsilon \qquad (3)$$

α is defined by $\alpha = k_BT/E_g$, where E_g is the energy gap between conduction and valence bands at L point. As shown in Fig. 5(a), at the same temperature, the Seebeck coefficients varied less than 10% among all compositions with different Sn contents ranging from 0% to 15%, which suggests the stabilization of Fermi level due to the similar doping level. However, the electrical conductivity was found to decrease remarkably with increasing Sn substitution (see Fig. 5(b)), revealing additional alloy scattering that contributed to the electrical transport process in $Pb_{1-x}Sn_xSe$ solid solutions. As shown in Fig. 5(c), at elevated temperatures the Sn substitution raised the power factor by ~10% for the samples with $x \leq 0.1$, but a higher Sn content caused a significant drop of electrical conductivity as compared in Fig. 5(d). The Sn substitution first significantly increased electrical conductivity in spite of a slight drop of thermopower for the Sn1% sample, which contributed to the power factor enhancement. However,
as shown in Fig. 5(d), changes both in electrical conductivity and Seebeck coefficient became smaller with increasing Sn content, and finally the electrical conductivity of the Sn15% sample turned to be lower than that of pristine PbSe. The mechanisms for such changes can be associated with the following Hall measurement results.

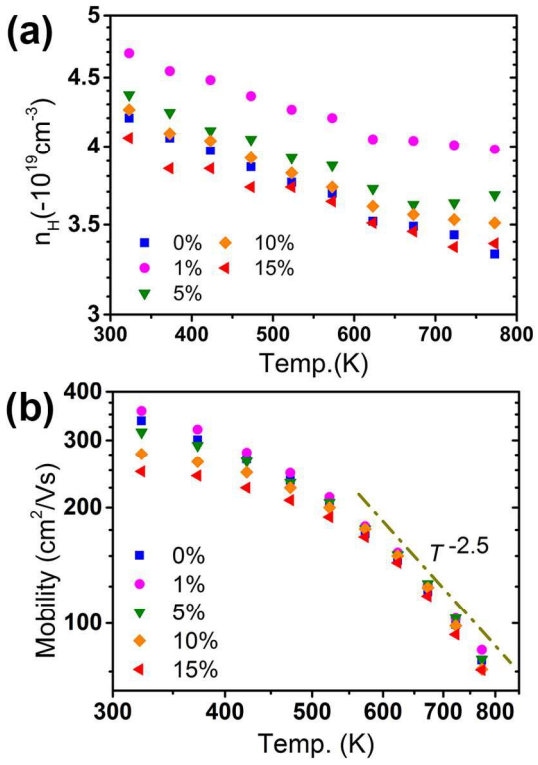

Fig. 6 (a) Hall carrier density and (b) mobility of all $Pb_{1-x}Sn_xSe$ compositions.

Figures 6(a)-(b) show the Hall carrier density and mobility of all $Pb_{1-x}Sn_xSe$ compositions. The room-temperature carrier density for all samples is 4~5×10^{19} cm^{-3}, since the Cl doping fraction was fixed at 0.2%, an optimized doping level according to a previous study on Cl-doped PbSe.[27] For each sample, the carrier density decreased with increasing temperature, which could be expected from a slight loss of degeneracy as temperature is raised.[19] As depicted in Fig. 6(b), the Sn substitution significantly suppressed the carrier mobility at low temperatures. In fact, in the range of 300-500K, the temperature dependency of carrier mobility varied from T^{-1} to $T^{-0.5}$ as the Sn content is increased, indicating the enhanced scattering from atomic disorder alloying effect. As temperature is raised, the mobility of different samples turned out to converge due to the domination of acoustic phonon scattering, in which the mobility behaved as $T^{-2.5}$.

It is interesting to note that the carrier density increased obviously when a small amount of Sn was added to form dilute $Pb_{1-x}Sn_xSe$ solid solutions, as shown in Fig. 7(a). In addition, when the Sn substitution was further increased, the carrier density suffered a slight decrease. Previous studies on dilute $Pb_{1-x}Sn_xSe$ solid solutions also revealed similar results but the mechanism was not yet confirmed.[35,36] Figure 7(b) displays the Hall measurements on Sn-free PbSe samples with various Cl doping fractions, indicating that the doping efficiency of Cl into PbSe was almost 100% ($\Delta n/\Delta n_{Cl} \approx 1$), and the Se vacancy concentration caused by excessive Pb was estimated to be 6×10^{18}cm^{-3}. Accordingly, in 0.2% Cl-doped $Pb_{1-x}Sn_xSe$ samples shown in Fig. 7(a), the majority of carrier density contributed by electrons originating from Cl substitution could be estimated to be almost the same as Cl concentration, with a value of 3.5×10^{19}cm^{-3}, while the rest (4~11×10^{18}cm^{-3}) was deduced to be associated with anionic Se vacancies that could generate more electrons by the defect reaction $V_{Se}^X \rightarrow V_{Se}^{\cdot\cdot} + 2e$. Hence, a possibility for the dramatic change in measured carrier densities of Cl-doped $Pb_{1-x}Sn_xSe$ (Fig. 7(a)) was suggested as the Sn-induced self-compensation. In other words, when Sn substitution was sufficiently low (for instance, x = 0.01 in the present work), the generation of anionic Se vacancies would be enhanced in order to compensate for the lattice strain caused by the considerable discrepancy in lattice constants of cubic SnSe (5.99Å, data taken from epitaxially grown thin films[37]) from PbSe (6.12Å, PDF#06-0354), which is also consistent with the XRD results. That is, the formation energy of Se vacancies was lowered by a small amount of Sn substitution at first, thus leading to a sudden increase in carrier density, as can be seen from Fig. 7(a). Further Sn substitution was found to reduce the total carrier density monotonously, which might be evolved in two independent ways:

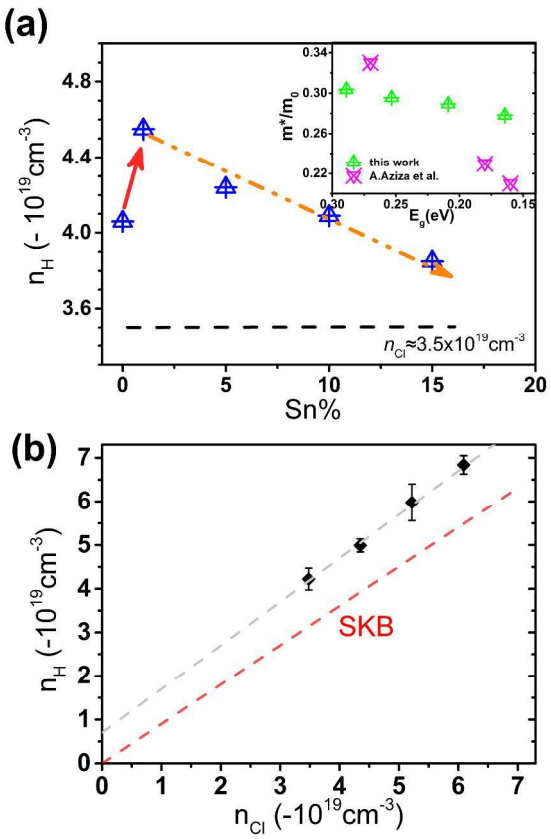

Fig. 7 (a) Hall carrier density as a function of Sn content at 373K, with the inset showing calculated *m** values by SKB model in this work and experimental values in ref.39 versus the band gap. (b) Hall carrier density of $Pb_{1.04}Se_{1-y}Cl_y$ samples as a function of Cl concentration. The red dash line represents the calculated carrier density based on SKB model.

First, the anionic Se vacancies initially created got filled up by Se atoms when more Sn was involved. Although the vacancy formation energy for a Se vacancy was lowered when the Sn substitution was quite small, the vacancies increased as more Sn atoms were present in the neighborhood, as a result of the stronger bonding of Sn-Se than Pb-Se due to the larger discrepancy in electronegativity between cationic and anionic atoms.

Second, the effective mass of electrons became smaller as the band gap was decreased almost linearly with increasing Sn substitution, which was demonstrated both by theoretical calculations[38] and experimental measurements in undoped n-type $Pb_{1-x}Sn_xSe$ alloys.[39] With the Fermi levels estimated from Seebeck data and Hall measurements, the variation of effective mass in the present work was calculated by the SKB model on the basis of following relations:

Carrier density: $$n = \frac{(2m^* k_B T)^{3/2}}{3\pi^2\hbar^3} {}^0F_0^{3/2} \qquad (4)$$

Hall carrier density: $$n_H = n/A \qquad (5)$$

Hall factor: $$A = \frac{3K(K+2)}{(2K+1)^2} \frac{{}^0F_{-4}^{1/2}\,{}^0F_0^{3/2}}{\left({}^0F_{-2}^{1}\right)^2} \qquad (6)$$

$K = m_\parallel^*/m_\perp^*$ (for PbSe, K=1.75, ignoring T dependency), as displayed in inset of Fig. 7(a), revealing a weaker dependency on the band gap (or Sn content) than that of undoped $Pb_{1-x}Sn_xSe$ samples[39] with measured carrier concentration in the range of 1.8~5.8×10^{19}cm^{-3}. These results suggested a possibility that the Fermi level moved deeply into the conduction band in strongly degenerate situation. As a result, the electrons on Fermi surfaces are far from the band extremum, being less influenced by the narrowing band gap as well as the stronger interaction between the conduction and valence bands.

The total and lattice thermal conductivities (κ and κ_L) as functions of temperature are shown in Fig. 8(a). The room-temperature κ values decreased with increasing amount of Sn, except for the pristine one which was comparable with the Sn5% sample. At elevated temperatures, the total thermal conductivity of all compositions reached ~1.3 W/mK, slightly higher than Br-doped n-type PbSe[29] with similar carrier density. The Lorentz number can be estimated by the SKB model:

$$L = \left(\frac{k_B}{e}\right)^2 \left[\frac{{}^2F_{-2}^1}{{}^0F_{-2}^1} - \left(\frac{{}^1F_{-2}^1}{{}^0F_{-2}^1}\right)^2\right] \qquad (7)$$

Assuming the acoustic phonon scattering domination and ignoring the bipolar diffusion, the lattice thermal conductivity is determined by the equation $\kappa_L = \kappa - L\sigma T$. Generally, the κ_L values for most samples are almost the same, especially at elevated temperatures, with a value of 0.7 W/mK at 700K, seemingly lower than the previously reported κ_L value for n-type PbSe[29] (about 0.8W/mK at 850K), which was likely to benefit from the refined grains and crystal defects derived by MA and SPS.

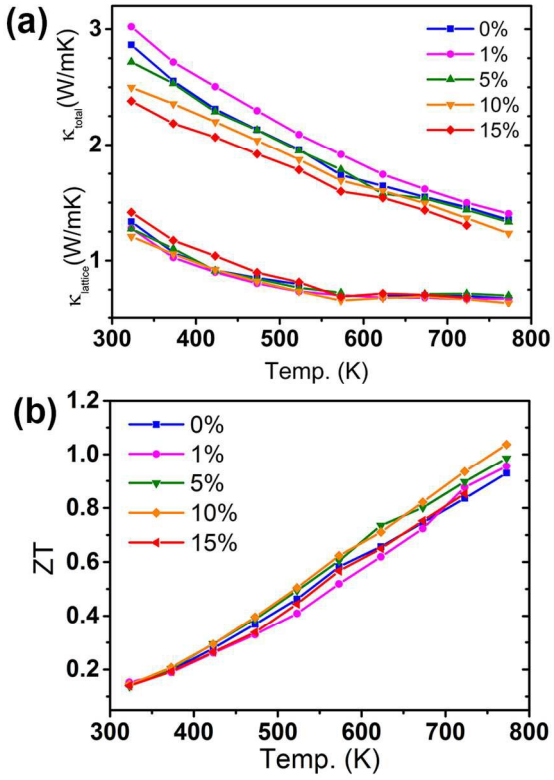

Fig. 8 (a) Total thermal conductivity and lattice thermal conductivity as a function of temperature. (b) *ZT* of 0.2%Cl-doped $Pb_{1-x}Sn_xSe$ solid solution materials.

Figure 8(b) presents the *ZT* values of $Pb_{1-x}Sn_xSe$ solid solutions as a function of temperature. Due to a balanced combination of power factors and thermal conductivity, the $Pb_{0.9}Sn_{0.1}Se$ composition shows the highest ZT value, especially at high temperatures. A maximum value up to 1.0 was obtained at 773K, but higher ZT values are expectable if measured at higher temperatures. It should be pointed out that the ZT enhancement was quite limited in $Pb_{1-x}Sn_xSe$ compared to the pristine PbSe, mainly because the formation of solid solutions has little alteration on host conduction band that governs the electrical transport process in n-type semiconductors. In addition, the present study revealed a possibility to reduce Pb contents of PbSe-based thermoelectric materials since the thermoelectric properties did not drop down even with Sn substitution up to 15%. Although *ZT* in this work is lower than the state-of the-art n-type nanostructured PbSe,[40] it is positively expected that further enhancement should be achieved in this promising system by proper band engineering and/or nanostructuring strategies.

4 Conclusions

In summary, solid solutions between PbSe and SnSe were fabricated by a process combining mechanical alloying and spark plasma sintering. Small amounts of Sn substitution for Pb lead to a moderate increase in carrier density. As a result, the power factor was increased by 10% in $Pb_{1-x}Sn_xSe$ when $x \leq 0.1$ compared to PbSe since the electrical conductivity is increased with no obvious decrease in Seebeck coefficient. A high ZT value up to 1.0 at a moderate temperature of 773K was obtained in the composition of $Pb_{0.9}Sn_{0.1}Se$. Although within the investigated range the composition of $Pb_{0.9}Sn_{0.1}Se$ shows the highest thermoelectric figure of merit at high temperatures, the differences in *ZT* values among these compositions are quite small. Further *ZT* enhancement can be expected by reducing thermal conductivity via nanostructuring in addition to band engineering doping.

Acknowledgements

This work was supported by the National Basic Research Program of China (Grant No. 2013CB632503) and the National Natural Science Foundation (No. 51172121) as well as the 863 Program under Grant No. 2012AA051104.

Notes and references

[a] State Key Laboratory of New Ceramics and Fine Processing, School of Materials Science and Engineering, Tsinghua University, Beijing, 100084, China.

1 L. E. Bell, *Science*, 2008, **321**, 1457-1461.
2 J. R. Sootsman, D. Y. Chung and M. G. Kanatzidis, *Angew. Chem. Int. Edit.*, 2009, **48**, 8616-8639.
3 G. J. Snyder and E. S. Toberer, *Nat. Mater.*, 2008, **7**, 105-114.
4 J.-F. Li, W. S. Liu, L. D. Zhao and M. Zhou, *NPG Asia Mater.*, 2010, **2**, 152-158.
5 S. V. Kershaw, A. S. Susha and A. L. Rogach, *Chem. Soc. Rev.*, 2013, **42**, 3033-3087.
6 S. A. Lourenco, N. O. Dantas and R. S. Silva, *Phys. Chem. Chem. Phys.*, 2012, **14**, 11040-11047.
7 E. G. Evola, M. D. Nielsen, C. M. Jaworski, H. Jin and J. P. Heremans, *J. Appl. Phys*., 2014, **115**, 0537045.
8 J. M. Skelton, S. C. Parker, A. Togo, I. Tanaka and A. Walsh, *Phys. Rev. B,* 2014, **89**, 20520320.
9 L. D. Zhao, V. P. Dravid and M. G. Kanatzidis, *Energy Environ. Sci.*, 2014, **7**, 251-268.
10 Y. M. Han, Z. Chen, C. N. Xin, Y. Z. Pei, M. Zhou, R. J. Huang and L. F. Li, *J. Alloy. Compd.*, 2014, **600**, 91-95.
11 H. T. Fan, T. C. Su, H. T. Li, Y. J. Zheng, S. S. Li, M. H. Hu, Y. M. Zhou, H. A. Ma and X. P. Jia, *Solid State Commun.*, 2014, **186**, 8-12.
12 E. O. Wrasse, P. Venezuela and R. J. Baierle, *J. Appl. Phys.*, 2014, **116**, 18.
13 J. Q. He, L. D. Zhao, J. C. Zheng, J. W. Doak, H. J. Wu, H. Q. Wang, Y. Lee, C. Wolverton, M. G. Kanatzidis and V. P. Dravid, *J. Am. Chem. Soc.*, 2013, **135**, 4624-4627.
14 Y. Lee, S. H. Lo, J. Androulakis, C. I. Wu, L. D. Zhao, D. Y. Chung, T. P. Hogan, V. P. Dravid and M. G. Kanatzidis, *J. Am. Chem. Soc.*, 2013, **135**, 5152-5160.
15 D. Parker, D. J. Singh, Q. Y. Zhang and Z. F. Ren, *J. Appl. Phys.*, 2012, **111**, 12370112.
16 Y. L. Pei and Y. Liu, *J. Alloy. Compd.*, 2012, **514**, 40-44.
17 J. Androulakis, Y. Lee, I. Todorov, D. Y. Chung and M. Kanatzidis, *Phys. Rev. B*, 2011, **83**, 19520919.
18 S. A. Yamini, H. Wang, Z. M. Gibbs, Y. Z. Pei, S. X. Dou and G. J. Snyder, *Phys. Chem. Chem. Phys.*, 2014, **16**, 1835-1840.
19 A. D. LaLonde, Y. Z. Pei and G. J. Snyder, *Energy Environ. Sci.*, 2011, **4**, 2090-2096.
20 R. Basu, S. Bhattacharya, R. Bhatt, M. Roy, S. Ahmad, A. Singh, M. Navaneethan, Y. Hayakawa, D. K. Aswal and S. K. Gupta, *J. Mater. Chem. A*, 2014, **2**, 6922-6930.
21 T. J. Zhu, H. L. Gao, Y. Chen and X. B. Zhao, *J. Mater. Chem. A*, 2014, **2**, 3251-3256.
22 H. Wang, J. L. Wang, X. L. Cao and G. J. Snyder, *J. Mater. Chem. A*, 2014, **2**, 3169-3174.
23 H. Wang, A. D. LaLonde, Y. Z. Pei and G. J. Snyder, *Adv. Funct. Mater.*, 2013, **23**, 1586-1596.
24 H. Wang, Z. M. Gibbs, Y. Takagiwa and G. J. Snyder, *Energy Environ. Sci.*, 2014, **7**, 804-811.
25 S. Charar, A. Obadi, C. Fau, M. Averous, V. D. Ribes, S. D. Corso, B. Liautard, J. C. Tedenac and S. Brunet, *Int. J. Infrared Milli.*, 1996, **17**, 365-374.
26 A. J. Strauss, *Phys. Rev.*, 1967, **157**, 608.
27 G. Alekseeva, E. Gurieva, P. Konstantinov, L. Prokofeva and M. Fedorov, *Semiconductors*, 1996, **10**, 1320.
28 I. U. I. Ravich, B. A. Efimova and I. A. Smirnov, *Semiconducting Lead Chalcogenides*, Plenum Press, New York, 1970.
29 H. Wang, Y. Z. Pei, A. D. LaLonde and G. J. Snyder, *Proc. Natl. Acad. Sci. USA*, 2012, **109**, 9705-9709.
30 V. P. Zlomanov, W. B. White and R. Roy, *Metall. Trans.*, 1971, **2**, 121.
31 R. Fritts, *Thermoelectric Materials and Devices*, Reinhold Pub. Corp, New York, 1960.
32 R. Blachnik and R. Igel, *Z. Naturforsch. B*, 1974, **29**, 625.
33 H. W. Peng, J. H. Song, M. G. Kanatzidis and A. J. Freeman, *Phys. Rev. B*, 2011, **84**, 12520712.

34 P. Dziawa, B. J. Kowalski, K. Dybko, R. Buczko, A. Szczerbakow, M. Szot, E. Lusakowska, T. Balasubramanian, B. M. Wojek, M. H. Berntsen, O. Tjernberg and T. Story, *Nat. Mater.*, 2012, **11**, 1023-1027.
35 A. N. Veis and N. A. Suvorova, *Semiconductors*, 1998, **32**, 397-400.
36 J. C. Ramage, R. A. Stradling, A. Aziza and M. Balkanski, *J. Phys. C: Solid State Phys.*, 1975, **8**, 1731.
37 N. S. Dantas, A. F. Da Silva and C. Persson, *Opt. Mater.*, 2008, **30**, 1451-1460.
38 P. J. Lin and L. Kleinman, *Phys. Rev.*, 1966, **142**, 478.
39 A. Aziza, E. Amzallag, M. Balkansk, *Solid State Commun*., 1970, **8**, 873.
40 Y. Lee, S. H. Lo, C. Q. Chen, H. Sun, D. Y. Chung, T. C. Chasapis, C. Uher, V. P. Dravid and M. G. Kanatzidis, *Nat. Commun.*, 2014, **5**, 3640.